CHEMISTRY OF MATERIALS

pubs.acs.org/cm

Article

Elucidation of Parasitic Reaction Mechanisms at Interfaces in Na−O_2 Batteries

Alex Von Gunten, Kunal Velinkar, Eranda Nikolla,* and Jeffrey Greeley*

Cite This: *Chem. Mater.* 2023, 35, 5945−5952

Read Online

ACCESS | Metrics & More | Article Recommendations | Supporting Information

ABSTRACT: Sodium-containing batteries have the potential to address many of the challenges faced in the ongoing development of enhanced energy storage devices. Sodium is inexpensive and earth abundant, and aprotic Na−O_2 batteries, in particular, have gravimetric energy densities significantly exceeding those of Li-ion devices. However, poor functional cell lifespans present a significant obstacle to the development of Na−O_2 cells, with parasitic side reactions involving the NaO_2 discharge products, leading to a rapid decline in cell performance. These parasitic reactions are hypothesized to occur through two main pathways: (i) deleterious dissolution of NaO_2 into the electrolyte during periods of cell idling and (ii) disproportionation of NaO_2 in the near-surface region to form Na-rich species ($Na_{1+x}O_2$) on the cathode. To formulate practical strategies to suppress these processes, in turn, the development of fundamental, molecular-level mechanistic understanding is essential. In this contribution, such mechanistic insights are elucidated by coupling density functional theory calculations with experimental observations to study the surface chemistry of the NaO_2 discharge product. First, a series of *ab initio* surface phase diagrams are constructed to determine the structure of the NaO_2 surfaces under realistic operating conditions, whereby an inverse relationship between surface coordination and surface energy is determined. Next, a molecular surface dissolution analysis is performed for the identified surface terminations, demonstrating a further inverse relationship between surface energy and the thermodynamic barrier for dissolution. Finally, a study of the thermodynamics of thin-film formation of sodium oxides over the NaO_2 discharge product is carried out and suggests that an electrochemical reduction reaction, rather than an inherent chemical disproportionation, forms the observed Na-rich species in the near-surface region under high discharge overpotentials. From these insights, we suggest future studies that may yield practical design changes to improve stability and extend the lifespan of Na−O_2 batteries.

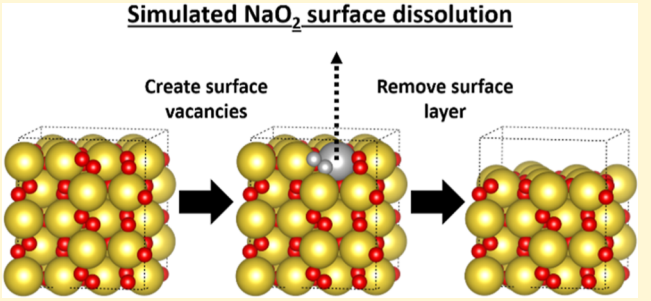

1. INTRODUCTION

The need to develop non-polluting, renewable energy resources has driven remarkable recent developments in energy storage technology. While lithium-ion (Li-ion) chemistry has revolutionized battery technology, Li-ion batteries are rapidly approaching their thermodynamic limits for gravimetric energy density. Promising alternative battery chemistries, with theoretical energy densities significantly exceeding those of Li-ion batteries, are the aprotic alkali metal-O_2 batteries (Li−O_2/Na−O_2).[1−3] Among these, Na−O_2 batteries present intriguing opportunities, given the greater elemental abundance of sodium, the associated low overpotential losses, and the possibility of using aluminum current collectors instead of costly copper collectors. In addition, they are relatively unexplored compared to Li−O_2 batteries.[2,4−6]

A Na−O_2 cell consists of a Na-metal anode, where Na-metal is oxidized upon discharge to Na^+ ions, and a porous carbon cathode, where Na^+ ions recombine with electrons to reduce O_2 gas from the ambient environment. In these systems, sodium superoxide (NaO_2), formed via a single electron transfer, has been observed as the major bulk discharge product.[7,8] It has been proposed that the relatively low surface energies of NaO_2, as compared to those of sodium peroxide (Na_2O_2), facilitate the nucleation and growth of the NaO_2 phase, even though Na_2O_2 is the most thermodynamically favorable bulk stoichiometry under electrochemical operating conditions.[7,9]

The physical structure of the NaO_2 discharge product is closely tied to the nature of the liquid electrolyte used in the Na−O_2 cell. A key parameter in this regard has been proposed to be the electrolyte donor number (DN), with high DN electrolytes (such as diethylene glycol dimethyl ether—DEGDME) resulting in the growth of micrometer-sized cubes on the cathode, and low DN electrolytes (such as

Received: April 11, 2023
Revised: July 11, 2023
Published: July 26, 2023

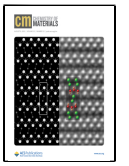

https://doi.org/10.1021/acs.chemmater.3c00850
Chem. Mater. 2023, 35, 5945−5952

tetra ethylene glycol dimethyl ether—TEGDME) resulting in thin film growth covering the cathode surface.[8] After discharge, subsequent charging of the Na−O_2 cell reverses the preceding electrochemical reactions, evolving O_2 gas back to the ambient environment and redepositing Na-metal on the anode.[4] For practical cell operation, the stability under periods of idling (held in a discharged state with no applied current), as well as the reversibility of the electrochemical reactions under cycling, are of paramount importance. However, rapid loss of cell performance has been observed under both idling and cycling conditions. The development of molecular-level mechanistic understanding of, and practical solutions for, these challenges has, in turn, remained elusive.[5,6,10,11]

The rapid decline in Na−O_2 cell performance has been partially attributed to an instability of the NaO_2 discharge product on the cathode.[5,6,10−12] Under idling conditions, NaO_2 is observed to continually dissolve from the cathode into the electrolyte. Scanning electron micrograph imaging from Kim et al. shows that NaO_2 cubes are preferentially etched along the edges, rather than on the cube faces, suggesting the preferential contribution of undercoordinated surface features to this parasitic dissolution.[6] The resulting solvated NaO_2 product (Na^+ and O_2^-) can, subsequently, undergo undesirable reactions with the electrolyte to form side products, such as $Na_2O_2{\cdot}2H_2O$, that degrade the cell performance. Conversely, upon cycling, the NaO_2 discharge product is observed to undergo parasitic disproportionation, leading to the accumulation of Na-rich oxide species ($Na_{1+x}O_2$) on the cathode. Combined X-ray diffraction and X-ray photoelectron spectroscopy (XPS) studies after discharge suggest that it is the near-surface region of the NaO_2 discharge product that undergoes disproportionation to form the Na-rich species.[12] A fraction of the Na-rich species formed at the cathode is, in turn, hypothesized to remain on the surface at the end of the charge cycle, and the resulting accumulation is suggested to contribute toward the observed decline in cell performance with extended cycling.

In spite of the importance of surface chemistry in governing these deleterious processes, studies of the molecular-level surface features of NaO_2 discharge products are substantially less well-developed than are similar analyses of the lithium superoxide and peroxide (LiO_2 and Li_2O_2, respectively) surfaces relevant for Li−O_2 battery chemistry.[7,13−17] First-principles studies of NaO_2 surface terminations have shown the (100) facet to be the most thermodynamically stable, giving rise to a predicted cubic crystal shape from a Wulff construction, consistent with observations of the NaO_2 discharge product formed in high DN electrolytes.[7,17] This result suggests, in turn, that the NaO_2 discharge product formed on the cathode in low DN electrolytes is kinetically trapped in a film-like geometry and cannot reconstruct to form the ground-state cubic crystal shape. However, in spite of the general agreement between the predicted Wulff shape and the observed particle shapes, the discharge product surface chemistry remains incompletely understood, and a comprehensive examination of the effect of surface layer stoichiometry, as well as surface defects, on the surface chemistry of the NaO_2 discharge product is needed to elucidate the molecular-level mechanisms by which parasitic reactivity occurs.

To provide molecular-level insights into the above phenomena, we study the surface chemistry of NaO_2 discharge products by first constructing density functional theory (DFT)-based surface phase diagrams. These diagrams, in turn, point to a representative set of surface features, including terraces, steps, and off-stoichiometric terminations, for use in subsequent studies of parasitic reactivity mechanisms under realistic electrochemical conditions. Next, an ab initio mechanistic surface dissolution analysis is implemented to probe the effect of surface coordination on the thermodynamics governing dissolution under conditions consistent with the early stages of idling in a Na−O_2 cell. From this analysis, a direct relationship between surface coordination number and the thermodynamic barrier for dissolution is observed, evidencing the preferential role that undercoordinated surface features play in the parasitic dissolution at the cathode.[6] Finally, to elucidate the surface thermodynamics governing the parasitic disproportionation in the near-surface region of the NaO_2 discharge product, we study the energetics of thin film formation of sodium oxide species over NaO_2 substrates under conditions consistent with discharge in a Na−O_2 cell. Compared to other sodium oxide film stoichiometries, Na_2O_2 films are found to be thermodynamically stable on (100)-NaO_2 substrates under high discharge overpotentials, suggesting that this species could form in the later stages of discharge.[12] We conclude by suggesting future work that may point to practical design changes to improve the stability and cyclability of Na−O_2 cells.

2. METHODS

2.1. Total Energy Calculations. Spin polarized, periodic density functional theory (DFT) calculations are performed with the Vienna *Ab Initio* Simulation Package (VASP, v5.4.1).[18−20] Converged energies and geometries are obtained through the minimization of the total energy with respect to geometry with all slab layers fully relaxed. Core electrons are treated using projector augmented-wave pseudopotentials with a plane wave cutoff energy of 500 eV.[21] Exchange−correlation effects are treated using the parametrization of the Bayesian error estimation functional with van der Waals interactions.[22] For bulk structures and surface slabs, a gamma-centered *k*-point grid of 8 × 8 × 8 and 2 × 2 × 1, respectively, is found to converge the total energies (see Supporting Information #1 for convergence criteria). Total energies are converged to values differing by less than 10^{-4} eV, and Hellmann−Feynman forces are minimized to values less than 0.02 eV/Å. Electronic occupancies are determined according to a Methfessel−Paxton scheme with an energy smearing of 0.2 eV.

Since experimental evidence suggests that pyrite-like NaO_2 is the primary discharge product formed in Na−O_2 cells, this structure is used as the basis for generating all surface slabs in this study.[7,23,24] All slabs are at least 7 Å in length in the directions parallel to the surface and have at least 4 surface-layer NaO_2 units. Surface slabs are at least 20 Å thick in the dimension perpendicular to the surface, with a vacuum spacing of at least 10 Å.

For the surface phase and dissolution analyses, possible defect-induced reconstructions of the surface geometry are explored using simulated annealing. In these analyses, all surface structures are annealed in AIMD simulations followed by DFT relaxations (quenching) of selected snapshots. In the AIMD runs, the top three surface layers are treated as dynamic while all other layers are fully constrained. Surface structures are temperature ramped to 500 K before being simulated in an *NVT* ensemble for 4 ps. Structures are selected for quenching every 400 fs. Additionally, at least five energy minima along the AIMD trajectory are selected for quenching. During quenching, all layers are allowed to fully relax, and the total energy is determined using the above parameters.

To simulate various sodium oxide films over (100)-NaO_2 substrates, multiple candidate film-substrate structures are generated for each film stoichiometry (Na_2O_2 or Na_2O) using an in-house lattice matching algorithm.[25,26] The algorithm populates different film-substrate combinations, of different unit cell sizes and orientations,

https://doi.org/10.1021/acs.chemmater.3c00850
Chem. Mater. 2023, 35, 5945−5952

such that the film orientation results in a minimal straining of the film. After generation, the film-substrate combination is allowed to fully relax, and the total energy is determined using the above parameters. Numerous film-substrate matches are considered for each stoichiometry, and only the most favorable matching is reported herein.

2.2. Thermodynamic Formalisms. To compare the favorability of various surface terminations, a thermodynamic formalism is adopted to compute the excess surface free energy, per unit area, resulting from cleaving a bulk NaO_2 crystal. Conditions consistent with cell idling are simulated with a grand canonical thermodynamic formalism, assuming that the surface slabs are quasi-equilibrated with bulk NaO_2 and an ambient O_2 gas reservoir at 300 K and 1 bar (see Supporting Information #2 for a discussion of the physical reasoning behind this choice of thermodynamic formalism). From these reservoirs, the surface excess free energy, normalized per unit area, is defined as

$$\gamma = \frac{1}{2A}[E_{slab} - N_{Na} \times (E_{NaO_2} - \mu_{O_2}) - N_{O_2} \times \mu_{O_2}] \quad (1)$$

where E_{slab} and E_{NaO_2} represent the DFT energies of the NaO_2 surface slab and NaO_2 bulk, respectively. For off-stoichiometric terminations, E_{slab} is corrected for the loss or gain of zero-point energy (ZPE) arising from either an O_2 vacancy or excess O_2, respectively (see Supporting Information #3 for a discussion of the ZPE treatment). The gas phase O_2 chemical potential (μ_{O_2}) is computed as

$$\mu_{O_2} = E_{O_2} + E_{ZPE} + \Delta H_{O_2}^{0-300K} - TS_{O_2}^{300K} \quad (2)$$

where E_{O_2} represents the DFT energy of an isolated O_2 molecule, corrected using the approach of Ceder et al. (see Supporting Information #4 for details of the correction to the O_2 gas phase chemical potential),[7] E_{ZPE} is the zero point energy of the isolated O_2 molecule, and $\Delta H_{O_2}^{0-300K}$ and $S_{O_2}^{300K}$ represent finite temperature corrections to the enthalpy and entropy of O_2 gas, respectively, as obtained from the NIST-JANAF thermochemical tables.[7,27]

To probe the propensity of various surface features to undergo dissolution, a thermodynamic formalism is adopted to compare the energy penalties associated with removing different species from a pristine surface termination. This energy penalty is associated with the thermodynamic driving force for surface dissolution, and the dissolution energy is defined as the difference in slab energy between a perturbed slab, with species removed, and the most stable surface termination of the respective facet, accounting for the removed units of the surface going to their defined reservoirs. The removed Na, O_2, or NaO_2 units are assumed to be quasi-equilibrated with bulk NaO_2 and an O_2 gas reservoir, simulating idling conditions of a Na−O_2 cell where parasitic dissolution is observed

$$E_{Diss} = E_{slab}^{*} + [N_{Na}^{rem} \times (E_{NaO_2} - \mu_{O_2}) + N_{O_2}^{rem} \times \mu_{O_2}] - E_{slab}^{0} \quad (3)$$

where E_{slab}^{*} and E_{slab}^{0} represent the DFT energies of the perturbed surface slab and the corresponding most stable surface termination of that facet, respectively. For off-stoichiometric slabs, E_{slab}^{*} is corrected for the loss or gain of ZPE arising from either an O_2 vacancy or excess O_2, respectively. N_{Na}^{rem} and $N_{O_2}^{rem}$ represent the number of Na and O_2 units, respectively, that are removed to simulate the dissolution.

Lastly, to probe the observed disproportionation of the NaO_2 discharge product in the near-surface region, an alternative thermodynamic formalism is adopted to assess the stability of various sodium oxide films over (100)-NaO_2 substrates. To describe the experimentally observed voltage dependence, the change in Na chemical potential is expressed in terms of the voltage of the Na anode, allowing the phase diagram to be directly related to experimental conditions

$$\mu_{Na} = E_{Na}^{0} - eU_{Na/Na^+} \quad (4)$$

where E_{Na}^{0} represents the bulk Na-metal energy, and eU_{Na/Na^+} is the potential versus the Na/Na^+ anode. The surface slabs are, in turn, presumed to be quasi-equilibrated with an O_2 gas reservoir and the Na/Na^+ anode (see Supporting Information #5 for a discussion of the physical reasoning behind this choice of thermodynamic formalism). The film formation energy, normalized per unit area, is defined as

$$\Delta G_{film} = \frac{1}{A} \times (E_{film+subs} - E_{subs} - N_{O_2}^{film} \times \mu_{O_2} - N_{Na}^{film} \times \mu_{Na}) \quad (5)$$

where $E_{film+subs}$ and E_{subs} represent the DFT energies of the combined film-NaO_2 substrate and the NaO_2 substrate, respectively. The $E_{film+subs}$ is corrected to account for the gain in ZPE from accepting O_2 from the reservoir. N_{Na}^{film} and $N_{O_2}^{film}$ represent the number of Na and O_2 units in the film, respectively.

3. RESULTS AND DISCUSSION

In this section, we begin with a discussion of the surface thermodynamics of different single crystal facets of NaO_2, including both smooth terraces and lower coordinated defect structures that represent cube faces and edges, respectively, of the NaO_2 discharge product.

3.1. Surface Phase Analysis. To elucidate the fundamental surface thermodynamics of the NaO_2 discharge product, we consider the (100), (110), (111), and (210) facets of pyrite-NaO_2 (Figure 1), which represent the three unique low Miller index surface facets, along with a surface facet representative of a linear, step-like defect in a pristine NaO_2 termination, respectively. The (100) facet is a terrace consisting of layers with integer NaO_2 stoichiometry. As generated from the bulk structure, and when viewed from the sides, the O_2 dimers lie at an angle with respect to the surface normal. However, after AIMD simulation and subsequent quenching (see Methods section for details), these O_2 dimers rotate toward the direction parallel to the surface plane, with the movement being particularly pronounced in the near-surface region (see Supporting Information #6 for a discussion of the O_2 dimer orientations). The (110) facet is likewise a terrace, composed of layers of integer NaO_2 stoichiometry, albeit with a looser packing density, with average Na−Na nearest neighbor distances of 4.67 Å as compared to 3.90 Å on

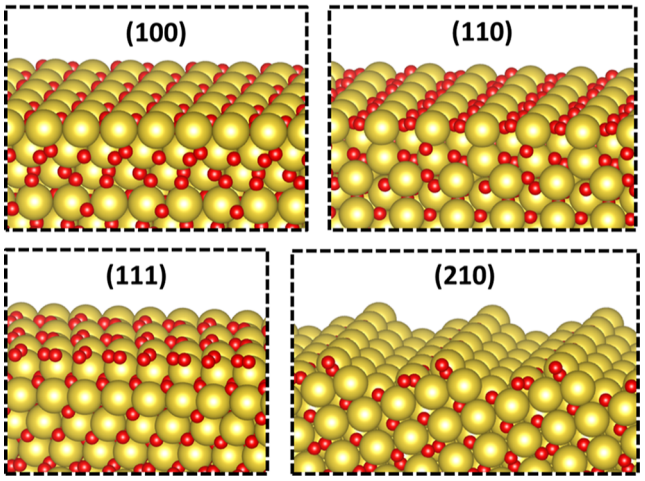

Figure 1. Visual representation of the geometries of the studied NaO_2 surface facets. The yellow spheres represent Na atoms, and the red spheres represent O atoms. All O atoms exist as a part of an O_2^- dimer.

https://doi.org/10.1021/acs.chemmater.3c00850
Chem. Mater. 2023, 35, 5945−5952

the (100) facet. In contrast, the (111) facet does not have layers of integer NaO_2 stoichiometry and consists of alternate O_2-rich and O_2-deficient layers. In this case, we identified the lowest energy stoichiometric structure by cleaving the slab at several points and carrying out AIMD relaxations of the resulting structures. The (111) stoichiometric termination was observed to significantly restructure, such that the O_2 dimers at the surface migrated to become incorporated between the first two layers of Na atoms. Finally, to represent undercoordinated surface features that may be present along a discharge product cube edge, the (210) facet is also considered. This facet consists of (100) terraces, three NaO_2 units in length, separated by periodic steps. In spite of the uncoordinated nature of the steps, the (210) terminations did not undergo restructuring during the AIMD simulation, as was seen with the (111) termination, suggesting that this could be a suitable model for a metastable defect on a (100) terrace.

The surface energies of the studied surface terminations are summarized in Figure 2a. In agreement with previous first-principles studies, the stoichiometric (100) termination is found to be the most thermodynamically favorable, while the stoichiometric (110), (111), and (210) terminations all show surface energies roughly double that of the (100) termination.[7,17] For the (100), (110), and (210) facets, a stoichiometric termination is the most stable. Further, all surface facets show a general preference for O_2-rich, as compared to O_2-deficient, terminations. The exception is the (111) facet, which shows nearly equivalent surface energies between the stoichiometric and mildly O_2-deficient terminations (we note that, with more than 1/2 ML of excess O_2, the O_2 dimers did not bind to the (111) surface). The general preference for stoichiometric surface terminations indicates that, under conditions consistent with idling, there is no inherent thermodynamic driving force to preferentially leach either Na or O_2 from the surface layers into the solution. Additionally, the surface energies of O_2 excess surfaces indicate that the discharge product surface is not predicted to be populated by physisorbed O_2 molecules. It is also worth noting that isolated oxygen atoms on the surface are found to be highly unstable and thus are not expected to contribute to the surface chemistry.

a)

	(meV/Å²)			
	(100)	(110)	(111)	(210)
1 ML O_2 vacancy	39	36	32	22
½ ML O_2 vacancy	24	23	14	18
Stoichiometric	7	17	15	14
½ ML O_2 excess	17	21	25	16
1 ML O_2 excess	29	28	----	19

Na-rich

O_2-rich

b)

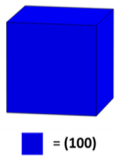

Figure 2. (a) Surface energies of NaO_2 surface terminations with varying levels of excess O_2 or O_2 vacancies. The (111) surface termination with more than 1/2 ML of excess O_2 is not stable (see text for details). (b) Wulff construction of the NaO_2 crystal determined from the surface energies in (a).

From the studied facets and their corresponding surface energies, a Wulff construction is used to predict the equilibrium crystal shape of the NaO_2 discharge product. The resulting shape is shown in Figure 2b. From the NaO_2 surface thermodynamics, the discharge product is predicted to be composed solely of (100) facets, giving rise to a cubic shape that is consistent with experimental observations when operating in high DN solvents.[8] However, while the Wulff construction predicts the equilibrium surface facets that are present on a crystal, it does not directly describe the contributions of edges and corners to the overall crystal thermodynamics. Such edges are nevertheless present on real crystals, and thus a population of defected terminations must exist along the edges of the NaO_2 discharge product cube. In our analysis, the less stable surface terminations studied and, in particular, the (210) step, may be representative of the surface chemistry of the NaO_2 discharge product at the cube edges.

Although the Wulff analysis provides a compact explanation for experimental results in high DN electrolytes, it is worth noting that there is a discrepancy between the Wulff predictions and the observed discharge product conformation in low DN electrolytes. There, the observation of a film of NaO_2, rather than a cube, is evidence that the discharge product is kinetically trapped on the cathode and is unable to reconstruct by dissolution and subsequent nucleation to take the equilibrium cubic shape. Instead, the discharge product film likely consists of an ensemble of surface terminations, governed by a competition between the relative kinetics of facet growth and the kinetics of surface reconstruction (diffusion of NaO_2 units along the surface to minimize surface free energy). Thus, in a low DN electrolyte, if the kinetics of surface reconstruction are sufficiently slow, and defected surface facets show preferential growth kinetics over the more stable (100) facets, then defected facets could play a greater role in governing the discharge product surface chemistry than in the case of a high DN electrolyte.

3.2. Mechanistic Analysis of Surface Dissolution.

Although the (100) facets dominate the cube surface of the NaO_2 discharge product, the undercoordinated cube edges could preferentially contribute to the observed parasitic dissolution under idling conditions. To assess this possibility, we analyze the effect of surface structure on the energetics of dissolution using a mechanistic molecular-level thermodynamic analysis. To compute the thermodynamic penalties associated with creating surface vacancies to undergo dissolution, we begin with a pristine surface termination, from which we remove a unit of the surface. The resulting surface vacancy is then relaxed using an AIMD simulation followed by quenching (see Methods section for details of the surface relaxation techniques). This procedure of removing a unit of the surface and relaxing the resulting slab is continued until a full layer of the surface has been removed, and the starting surface geometry is regenerated by symmetry. The removal of surface units, in turn, can occur through either a stoichiometric or an off-stoichiometric pathway, with the lowest energetic pathway indicative of the dissolution mechanism occurring under idling conditions. A stoichiometric pathway involves the removal of stoichiometric NaO_2 units and, conversely, an off-stoichiometric pathway involves the removal of Na atoms or O_2 dimers such that the surface becomes either O_2-rich or O_2-deficient, respectively. At each stage of the process, all possible permutations of surface removal for the chosen unit cells have been considered, but only the results of the most energetically favorable pathways are reported.

To compare the energetics of dissolution under idling conditions, a thermodynamic formalism (eq 3) is adopted such that the Na chemical potential is set by NaO_2 bulk, indicative of open circuit voltage conditions. We note that, while explicitly incorporating a liquid electrolyte in this analysis

https://doi.org/10.1021/acs.chemmater.3c00850
Chem. Mater. 2023, 35, 5945−5952

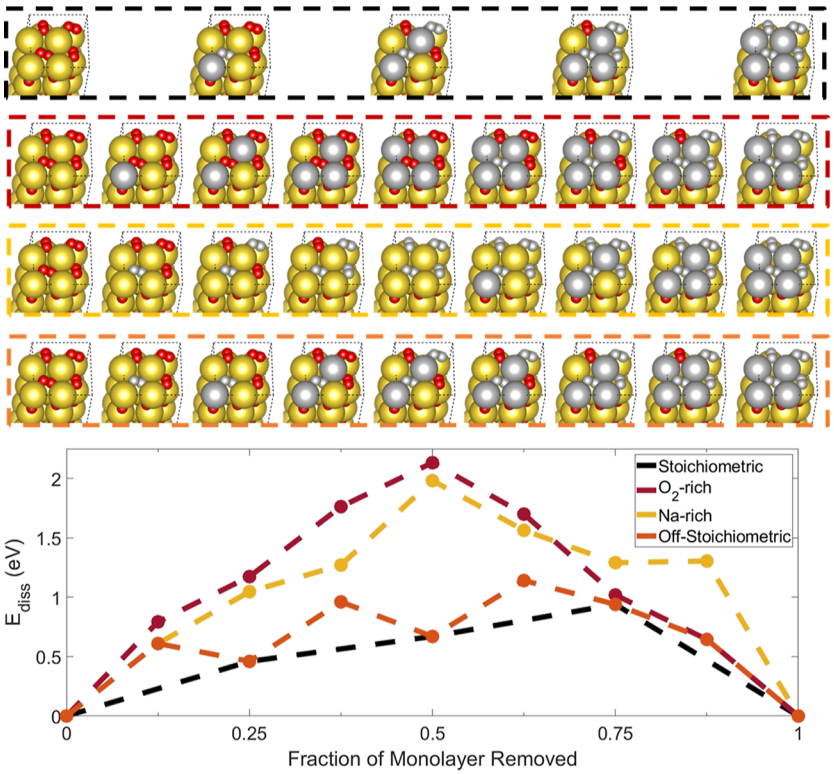

Figure 3. Energetics of the simulated dissolution of the (100) facet. The four considered pathways are: stoichiometric (black), O_2-rich (red), Na-rich (yellow), and minimum energy off-stoichiometric (orange) in which the NaO_2 stoichiometry is not enforced. Gray spheres correspond to vacancies.

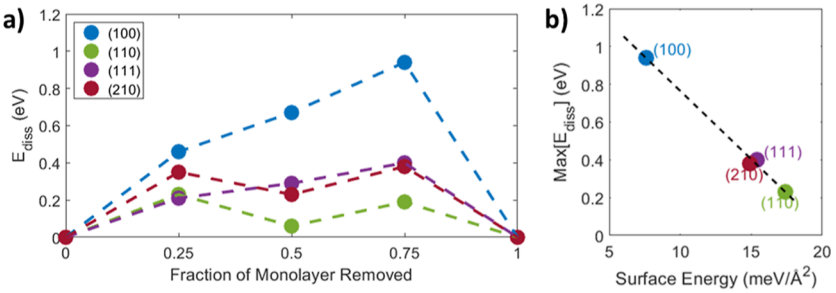

Figure 4. (a) Comparison of the dissolution energies of various NaO_2 surface facets (see Supporting Information #7 for geometric depictions of dissolution pathways), with a stoichiometric NaO_2 formula unit removed from the surface at each step along the reaction pathway. (b) The computed thermodynamic dissolution barrier compared to the surface energy of each NaO_2 facet studied.

would likely shift the absolute values of the dissolution energetics, the shift in the dissolution energetics from explicitly treating a liquid electrolyte is expected to be roughly constant across the various surface terminations. Thus, the qualitative trends in the thermodynamics of dissolution across the various surface facets can be captured using the current approach, variations of which have been extensively used to study dissolution and corrosion processes in the literature.[28−31]

The results of the simulated stoichiometric and off-stoichiometric dissolution of the (100) facet are summarized in Figure 3. For the stoichiometric removal of NaO_2 units, it is seen that the dissolution energy monotonically increases until reaching a maximum, corresponding to a single NaO_2 unit left on the surface. Further, although a wide configurational space is sampled in each case using the AIMD simulations, no obvious energetically favorable reconstructions of the surface vacancies are observed for the (100) facet. The O_2-rich pathway, whereby all Na atoms are first removed from the surface layer before subsequent removal of O_2 dimers, showed a thermodynamic penalty significantly greater than that of the stoichiometric NaO_2 pathway, consistent with the preference for stoichiometric slabs from the surface phase diagram. Similarly, the Na-rich pathway, whereby all O_2 dimers atoms were first removed from the surface layer before subsequent removal of Na atoms, showed an energetic penalty that was significantly greater than the stoichiometric pathway. The minimum energy off-stoichiometric pathway represents the minimum thermodynamic dissolution energy for the (100) facet in which the NaO_2 stoichiometry is not enforced. The results indicate that, once a Na atom or O_2 dimer has been removed from the surface layer, there is a preferential thermodynamic driving force to remove an O_2 dimer or Na atom, respectively, to restore the NaO_2 stoichiometry before the next vacancy is created. Thus, the most favorable off-stoichiometric pathway has behavior that closely tracks that of the stoichiometric pathway.

https://doi.org/10.1021/acs.chemmater.3c00850
Chem. Mater. 2023, 35, 5945−5952

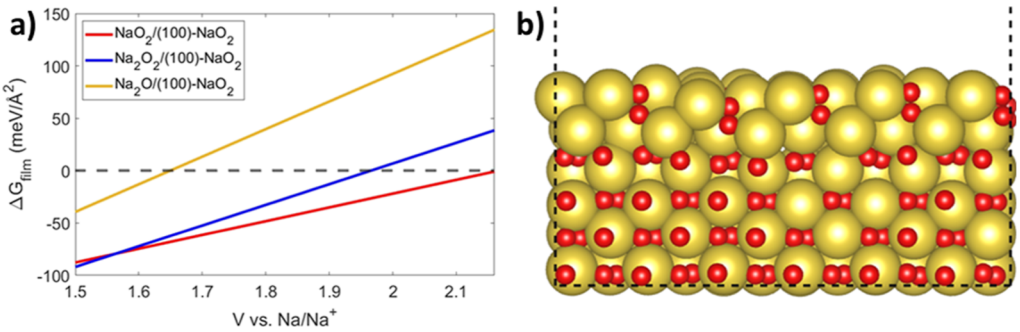

Figure 5. (a) Thermodynamics of the growth of the various sodium oxide films over (100)-NaO_2 substrates. At high discharge overpotentials (low potentials vs Na/Na^+), Na_2O_2 films growing on the NaO_2 substrates are found to be thermodynamically favorable. For the entirety of the potential window, Na_2O films are not thermodynamically favorable compared to NaO_2 or Na_2O_2 films. (b) Relaxed film-substrate combination of a Na_2O_2 film on a (100)-NaO_2 substrate. The top two layers are the Na_2O_2 film, and the bottom 4 layers are the (100)-NaO_2 substrate.

Given that the stoichiometric dissolution pathway is found to be the most energetically favorable for the (100) facet, we have analyzed a similar pathway on the other studied surface facets (Figure 4a). The (111) facet shows similar behavior to that of the (100) facet, with the dissolution energy increasing monotonically as NaO_2 units are removed, and the maximum dissolution energy corresponds to a single NaO_2 unit left on the surface. However, the (110) and (210) facets show a qualitatively different evolution of the dissolution energy. For these facets, rather than increasing monotonically, the dissolution energy behaves symmetrically along the reaction coordinate, passing through a local minimum corresponding to the removal of a half monolayer of the surface. This behavior can be rationalized by geometric arguments since, unlike the (100) and (111) facets, the (110) and (210) facets have a distinct row structure, with the removal of one complete row giving the intermediate local minimum, and removal of a second complete row returning the surface to its original state.

Taking the maximum of the E_{diss} along the reaction coordinate to be the thermodynamic barrier for a surface termination to undergo dissolution, we observe that the less intrinsically stable (higher surface energy) (110), (111), and (210) surface facets all show a thermodynamic barrier of less than one-half the barrier of the most stable (100) facet. From this analysis, an inverse relationship between the surface energy and the thermodynamic dissolution barrier is identified (Figure 4b). The trends of this analysis are fully consistent with the experimental observation of the preferential etching of the cube edges of the NaO_2 discharge product and clearly indicate that the driving force for the dissolution of the under-coordinated surface features is their high surface energy.[6] These trends suggest, in turn, the usefulness of passivating the cube edges of the NaO_2 discharge product to minimize the parasitic dissolution of the discharge product in $Na-O_2$ cells under idling conditions. A potential approach might involve the development of electrolyte additives that would preferentially bind to the NaO_2 discharge product cube edges during discharge and re-dissolve during subsequent charging.

3.3. Na-Rich Film Formation Analysis. While the performance decline with cycling in $Na-O_2$ cells has been attributed in part to the formation of various sodium oxides in the near-surface region of the electrode, the energetics of disproportionation of the NaO_2 discharge product remain unknown. Here, we study disproportionation at the surface of the NaO_2 discharge product to form Na-rich phases ($Na_{1+x}O_2$).[12] The disproportionation could, in turn, occur via two pathways: a further electrochemical reduction or a strictly chemical disproportionation. In the former case, the NaO_2 discharge product reacts with a Na^+ ion and an electron and is reduced to Na_2O_2, which could further undergo a reduction in the presence of Na^+ ions and electrons, leading to the formation of Na_2O at very high discharge overpotentials.[32] In contrast, in chemical disproportionation, two NaO_2 units could spontaneously react to form a Na_2O_2 unit and reject an O_2 unit to the gas phase. This process is energetically favorable in the bulk although further conversion to bulk Na_2O is endergonic under battery operating conditions. In either case, although the bulk thermodynamics are well known, it is entirely possible that the energetics of surface NaO_2, Na_2O_2, and Na_2O films may differ considerably from the corresponding bulk values, and conversion of surface or near-surface films is likely to be a precursor to any sort of longer-range bulk transformation. We therefore analyze this possibility in detail below.

To probe the energetics of the surface disproportionation, we performed a detailed analysis of the thermodynamics of Na-rich thin films over NaO_2 substrates (see Methods section for details of the thin film geometries). Since the (100) termination has the lowest surface energy and is predicted to dominate the cubic discharge product (Figure 2), it is chosen as the substrate for the sodium oxide films. In spite of the observed importance of the (210) step facet in the previous study of parasitic dissolution (Figure 4), the corrugated nature of the (210) facet likely prevents a favorable lattice matching with other sodium oxide phases and thus is not expected to form a stable film-substrate interface.

A voltage-dependent formalism is adopted to account for the operating voltage under conditions consistent with discharge at the anode of the $Na-O_2$ cell. To simulate the change in Na chemical potential with the change in cell voltage, the film-substrate slabs are assumed to be equilibrated with the Na/Na^+ anode and an O_2 gas reservoir. As such, the Na chemical potential is a function of the cell voltage (eq 4), allowing the thermodynamic predictions of this analysis to be directly compared with experiments. Bounds for the cell voltage are chosen to be 1.5 V versus Na/Na^+ (high discharge overpotential) and 2.16 V versus Na/Na^+ (equilibrium voltage, calculated). At the equilibrium voltage, the Na in solution is equilibrated with bulk NaO_2, which corresponds to the idling state used in the previous surface phase and dissolution analysis. As this analysis is purely thermodynamic in nature, it

https://doi.org/10.1021/acs.chemmater.3c00850
Chem. Mater. 2023, 35, 5945−5952

may be most directly applicable to the limit of slow transformation kinetics or low current densities.

For this analysis, only reactions between the NaO_2 discharge product, Na^+ ions, and dissolved O_2 molecules in the electrolyte are analyzed. We note that, upon idling of the cell, additional $Na_2O_2{\cdot}2H_2O$ can be formed, which is hypothesized to arise from a chemical reaction of the NaO_2 discharge product with the electrolyte.[6,10] However, since the formation of this species involves direct interactions between the discharge product and the electrolyte, we do not further analyze it here.

The energetics of film formation are summarized in Figure 5. For much of the potential window, the NaO_2 film on the (100)-NaO_2 substrate is the most stable species, suggesting that under modest overpotentials and idling conditions, the NaO_2 discharge product will not spontaneously disproportionate to other sodium oxide phases. However, the thermodynamic formation energy of the Na_2O_2 film becomes increasingly more competitive at higher discharge overpotentials, consistent with conditions at the later stages of discharge. Conversely, Na_2O is not found to be favorable on the (100)-NaO_2 substrate under reasonable cell voltages. The trends observed from the film formation energies confirm that the surface thermodynamics of the sodium oxides, particularly Na_2O_2, on NaO_2 substrates are distinct from the corresponding bulk thermodynamics. From surface thermodynamics, Na_2O_2 formation only becomes energetically favorable at much lower voltages than are required for the corresponding transition to occur in the bulk. This suggests that the thermodynamic driving force for the formation of Na_2O_2 in the near-surface region is a rise in the discharge overpotential, consistent with experimental XPS studies of the near-surface region of cathodes after discharge.[12] As such, it is evidenced that the discharge voltage of a Na−O_2 cell should be maintained near the thermodynamic voltage to avoid the formation and subsequent accumulation of Na-rich species on the cathode. Alternatively, cathode surface engineering might be used to selectively stabilize the NaO_2 discharge product and prevent the disproportionation and subsequent accumulation of Na-rich species.

4. CONCLUSIONS

Ab initio thermodynamic calculations are used to elucidate the parasitic mechanisms that degrade the performance of Na−O_2 battery cells. A comprehensive analysis of the surface thermodynamics and mechanisms of NaO_2 surface dissolution under idling demonstrates that undercoordinated surface features, such as those along NaO_2 cube edges, have roughly one-half the thermodynamic dissolution barrier of the most stable (100) facet on the cube faces. This result evidences the preferential role that undercoordinated surface features play in driving parasitic dissolution. Further, an exploration of the thermodynamics of Na-rich film formation over (100)-NaO_2 substrates suggests that the formation of Na_2O_2 films is thermodynamically favorable under high discharge overpotentials, indicating that the near-surface region of the NaO_2 discharge product may undergo further electrochemical reduction more readily under conditions consistent with the later stages of discharge, when a rise in the overpotential is observed. These mechanistic insights lay a foundation for future efforts to design mitigation strategies for parasitic degradation mechanisms in Na−O_2 batteries.

■ ASSOCIATED CONTENT

Supporting Information

The Supporting Information is available free of charge at https://pubs.acs.org/doi/10.1021/acs.chemmater.3c00850.

Convergence criteria, discussion of the physical reasoning for the idling state thermodynamic formalism, discussion of ZPE treatment (gas phase, surface adsorbed, and surface vacancy O_2 units), details of the correction to the O_2 gas phase chemical potential, discussion of the physical reasoning for the voltage-dependent thermodynamic formalism, discussion of the O_2 dimer orientations, geometries of stoichiometric surface dissolution pathways ((100), (110), (111), and (210)) (PDF)

■ AUTHOR INFORMATION

Corresponding Authors

Eranda Nikolla − *Department of Chemical Engineering, University of Michigan, Ann Arbor, Michigan 48109, United States;* orcid.org/0000-0002-8172-884X; Email: erandan@umich.edu

Jeffrey Greeley − *Davidson School of Chemical Engineering, Purdue University, West Lafayette, Indiana 47907, United States;* orcid.org/0000-0001-8469-1715; Email: jgreeley@purdue.edu

Authors

Alex Von Gunten − *Davidson School of Chemical Engineering, Purdue University, West Lafayette, Indiana 47907, United States*

Kunal Velinkar − *Department of Chemical Engineering, University of Michigan, Ann Arbor, Michigan 48109, United States*

Complete contact information is available at: https://pubs.acs.org/10.1021/acs.chemmater.3c00850

Author Contributions

The manuscript was written through the contributions of all authors. All authors have given approval to the final version of the manuscript.

Notes

The authors declare no competing financial interest.

■ ACKNOWLEDGMENTS

We gratefully acknowledge funding from the United States National Science Foundation under award numbers CBET-1935581 and CBET-1935645. A.V.G. and J.G. gratefully acknowledge the computational resources from the National Energy Research Scientific Computing Center.

■ REFERENCES

(1) Girishkumar, G.; McCloskey, B.; Luntz, A. C.; Swanson, S.; Wilcke, W. Lithium−Air Battery: Promise and Challenges. *J. Phys. Chem. Lett.* **2010**, *1*, 2193−2203.

(2) Kwak, W.-J.; Rosy; Sharon, D.; Xia, C.; Kim, H.; Johnson, L. R.; Bruce, P. G.; Nazar, L. F.; Sun, Y.-K.; Frimer, A. A.; Noked, M.; Freunberger, S. A.; Aurbach, D. Lithium−Oxygen Batteries and Related Systems: Potential, Status, and Future. *Chem. Rev.* **2020**, *120*, 6626−6683.

(3) Samira, S.; Deshpande, S.; Greeley, J.; Nikolla, E. Aprotic Alkali Metal−O $_2$ Batteries: Role of Cathode Surface-Mediated Processes and Heterogeneous Electrocatalysis. *ACS Energy Lett.* **2021**, *6*, 665−674.

(4) Hartmann, P.; Bender, C. L.; Vračar, M.; Dürr, A. K.; Garsuch, A.; Janek, J.; Adelhelm, P. A Rechargeable Room-Temperature Sodium Superoxide (NaO2) Battery. *Nat. Mater.* **2013**, *12*, 228−232.
(5) Black, R.; Shyamsunder, A.; Adeli, P.; Kundu, D.; Murphy, G. K.; Nazar, L. F. The Nature and Impact of Side Reactions in Glyme-Based Sodium-Oxygen Batteries. *ChemSusChem* **2016**, *9*, 1795−1803.
(6) Kim, J.; Park, H.; Lee, B.; Seong, W. M.; Lim, H.-D.; Bae, Y.; Kim, H.; Kim, W. K.; Ryu, K. H.; Kang, K. Dissolution and Ionization of Sodium Superoxide in Sodium−Oxygen Batteries. *Nat. Commun.* **2016**, *7*, 10670.
(7) Kang, S.; Mo, Y.; Ong, S. P.; Ceder, G. Nanoscale Stabilization of Sodium Oxides: Implications for Na−O $_2$ Batteries. *Nano Lett.* **2014**, *14*, 1016−1020.
(8) Lutz, L.; Yin, W.; Grimaud, A.; Alves Dalla Corte, D.; Tang, M.; Johnson, L.; Azaceta, E.; Sarou-Kanian, V.; Naylor, A. J.; Hamad, S.; Anta, J. A.; Salager, E.; Tena-Zaera, R.; Bruce, P. G.; Tarascon, J.-M. High Capacity Na−O $_2$ Batteries: Key Parameters for Solution-Mediated Discharge. *J. Phys. Chem. C* **2016**, *120*, 20068−20076.
(9) Bender, C. L.; Hartmann, P.; Vračar, M.; Adelhelm, P.; Janek, J. On the Thermodynamics, the Role of the Carbon Cathode, and the Cycle Life of the Sodium Superoxide (NaO_2) Battery. *Adv. Energy Mater.* **2014**, *4*, 1301863.
(10) Sun, Q.; Liu, J.; Xiao, B.; Wang, B.; Banis, M.; Yadegari, H.; Adair, K. R.; Li, R.; Sun, X. Visualizing the Oxidation Mechanism and Morphological Evolution of the Cubic-Shaped Superoxide Discharge Product in Na−Air Batteries. *Adv. Funct. Mater.* **2019**, *29*, 1808332.
(11) Qin, B.; Chan, K.-Y.; Li, C.-Y. V. Studies of Superoxide Degradation Kinetics and Electrolyte Management for a Reversible NaO $_2$ Battery. *ACS Sustain. Chem. Eng.* **2020**, *8*, 4317−4324.
(12) Jovanov, Z. P.; Lutz, L.; Lozano, J. G.; Holc, C.; Gao, X.; Grimaud, A.; Tarascon, J.; Chen, Y.; Johnson, L. R.; Bruce, P. G. Competitive Oxygen Reduction Pathways to Superoxide and Peroxide during Sodium-Oxygen Battery Discharge. *Batteries Supercaps* **2022**, *5*, No. e202200055.
(13) Hummelshøj, J. S.; Blomqvist, J.; Datta, S.; Vegge, T.; Rossmeisl, J.; Thygesen, K. S.; Luntz, A. C.; Jacobsen, K. W.; Nørskov, J. K. Communications: Elementary Oxygen Electrode Reactions in the Aprotic Li-Air Battery. *J. Chem. Phys.* **2010**, *132*, 071101.
(14) Seriani, N. Ab Initio Thermodynamics of Lithium Oxides: From Bulk Phases to Nanoparticles. *Nanotechnology* **2009**, *20*, 445703.
(15) Radin, M. D.; Rodriguez, J. F.; Tian, F.; Siegel, D. J. Lithium Peroxide Surfaces Are Metallic, While Lithium Oxide Surfaces Are Not. *J. Am. Chem. Soc.* **2012**, *134*, 1093−1103.
(16) Didar, B. R.; Yashina, L.; Groß, A. First-Principles Study of the Surfaces and Equilibrium Shape of Discharge Products in Li−Air Batteries. *ACS Appl. Mater. Interfaces* **2021**, *13*, 24984−24994.
(17) Lee, B.; Seo, D.-H.; Lim, H.-D.; Park, I.; Park, K.-Y.; Kim, J.; Kang, K. First-Principles Study of the Reaction Mechanism in Sodium−Oxygen Batteries. *Chem. Mater.* **2014**, *26*, 1048−1055.
(18) Kresse, G.; Furthmüller, J. Efficiency of Ab-Initio Total Energy Calculations for Metals and Semiconductors Using a Plane-Wave Basis Set. *Comput. Mater. Sci.* **1996**, *6*, 15−50.
(19) Kresse, G.; Hafner, J. *Ab Initio* Molecular Dynamics for Liquid Metals. *Phys. Rev. B: Condens. Matter Mater. Phys.* **1993**, *47*, 558−561.
(20) Kresse, G.; Furthmüller, J. Efficient Iterative Schemes for *Ab Initio* Total-Energy Calculations Using a Plane-Wave Basis Set. *Phys. Rev. B: Condens. Matter Mater. Phys.* **1996**, *54*, 11169−11186.
(21) Kresse, G.; Joubert, D. From Ultrasoft Pseudopotentials to the Projector Augmented-Wave Method. *Phys. Rev. B: Condens. Matter Mater. Phys.* **1999**, *59*, 1758−1775.
(22) Wellendorff, J.; Lundgaard, K. T.; Møgelhøj, A.; Petzold, V.; Landis, D. D.; Nørskov, J. K.; Bligaard, T.; Jacobsen, K. W. Density Functionals for Surface Science: Exchange-Correlation Model Development with Bayesian Error Estimation. *Phys. Rev. B: Condens. Matter Mater. Phys.* **2012**, *85*, 235149.
(23) Templeton, D. H.; Dauben, C. H. The Crystal Structure of Sodium Superoxide ^{1}. *J. Am. Chem. Soc.* **1950**, *72*, 2251−2254.
(24) Carter, G. F.; Templeton, D. H. Polymorphism of Sodium Superoxide. *J. Am. Chem. Soc.* **1953**, *75*, 5247−5249.
(25) Samira, S.; Deshpande, S.; Roberts, C. A.; Nacy, A. M.; Kubal, J.; Matesić, K.; Oesterling, O.; Greeley, J.; Nikolla, E. Nonprecious Metal Catalysts for Tuning Discharge Product Distribution at Solid−Solid Interfaces of Aprotic Li−O $_2$ Batteries. *Chem. Mater.* **2019**, *31*, 7300−7310.
(26) Zeng, Z.; Chang, K.-C.; Kubal, J.; Markovic, N. M.; Greeley, J. Stabilization of Ultrathin (Hydroxy)Oxide Films on Transition Metal Substrates for Electrochemical Energy Conversion. *Nat. Energy* **2017**, *2*, 17070.
(27) Chase, M. W. *NIST-JANAF Thermochemical Tables*, 4th ed.; American Chemical Society; American Institute of Physics for the National Institute of Standards and Technology: Washington, DC, 1998.
(28) Erlebacher, J.; Aziz, M. J.; Karma, A.; Dimitrov, N.; Sieradzki, K. Evolution of Nanoporosity in Dealloying. *Nature* **2001**, *410*, 450−453.
(29) Viswanathan, V.; Nørskov, J. K.; Speidel, A.; Scheffler, R.; Gowda, S.; Luntz, A. C. Li−O $_2$ Kinetic Overpotentials: Tafel Plots from Experiment and First-Principles Theory. *J. Phys. Chem. Lett.* **2013**, *4*, 556−560.
(30) Greeley, J. Structural Effects on Trends in the Deposition and Dissolution of Metal-Supported Metal Adstructures. *Electrochim. Acta* **2010**, *55*, 5545−5550.
(31) Siahrostami, S.; Tripković, V.; Lundgaard, K. T.; Jensen, K. E.; Hansen, H. A.; Hummelshøj, J. S.; Mýrdal, J. S. G.; Vegge, T.; Nørskov, J. K.; Rossmeisl, J. First Principles Investigation of Zinc-Anode Dissolution in Zinc−Air Batteries. *Phys. Chem. Chem. Phys.* **2013**, *15*, 6416.
(32) Bender, C. L.; Schröder, D.; Pinedo, R.; Adelhelm, P.; Janek, J. One- or Two-Electron Transfer? The Ambiguous Nature of the Discharge Products in Sodium-Oxygen Batteries. *Angew. Chem., Int. Ed.* **2016**, *55*, 4640−4649.

https://doi.org/10.1021/acs.chemmater.3c00850
Chem. Mater. 2023, 35, 5945−5952